The electronic structure of Pd-Pt random alloys: a relativistic KKR-CPA calculation

1989 J. Phys.: Condens. Matter 1 8385

(http://iopscience.iop.org/0953-8984/1/44/010)

J. Phys.: Condens. Matter 1 (1989) 8385–8396. Printed in the UK

The electronic structure of Pd–Pt random alloys: a relativistic KKR–CPA calculation

G M Florio†, B Ginatempo†, E S Giuliano† and J B Staunton‡

† Istituto di Fisica Teorica, Universita' di Messina, I-98166 Vill. S Agata (Messina), Italy

‡ Department of Physics, University of Warwick, Coventry CV4 7AL, UK

Received 13 June 1988, in final form 15 March 1989

Abstract. By applying a new method for solving the equations of the relativistic Korringa–Kohn–Rostoker–coherent-potential approximation, we have been able to study the electronic structure of compositionally disordered Pd–Pt alloys. This investigation was carried out, on the one hand, to test the reliability of the method itself and, on the other, to learn whether a 'rigid band' picture is appropriate for these alloys as suggested by an interpretation of residual resistivity measurements. We find that the method is numerically stable and can now be safely incorporated into a self-consistent-field, local-density theory for alloys with heavy elements. Moreover, the electronic structure of Pd–Pt is found to be 'non-rigid-band' like and demonstrates some interesting new features arising from mass–velocity, Darwin and spin–orbit coupling effects.

1. Introduction

Following the implementation of the so called SCF–KKR–CPA method (Stocks and Winter 1982) the electronic structure of random alloys can be studied in terms of a 'first principles' theory and its role in determining many of the physical properties of such an important class of materials has begun to be quantitatively understood (Stocks and Gonis 1989). This has led to the development of efficient codes which incorporate charge self-consistency within the local density functional approximation as well as scattering self-consistency specified by the KKR–CPA (Johnson *et al* 1984). Consequently it is now possible to study the influence of the alloying on electronic states to high level of accuracy and therefore, to deal with fundamental problems of alloy physics. As a matter of fact, total energy calculations (Gyorffy *et al* 1989), and the suggestion that Fermi-surface topology can be a relevant parameter in driving order–disorder transitions (Wadsworth *et al* 1985), represent only a few examples of the success obtained using this modern theory of alloys (see, e.g., Stocks and Gonis 1989). Until recently, however, the results obtained for alloys containing heavy elements remained on a less firm basis than that for 'light alloys ($Z \leqslant 50$). The reasons for that were due to the lack of a reliable numerical solution of the relativistic KKR–CPA(RKKR–CPA) equations. Efforts to solve the Dirac problem in a random alloy along the lines followed in the Schrödinger counterpart were not always satisfactory and, to our knowledge, no solution has been found for Pd–Pt alloys.

In a previous paper (Ginatempo and Staunton 1988, hereafter referred to as I) the problem of solving the RKKR–CPA equations numerically was critically reviewed and a

0953-8984/89/448385 + 12 $02.50

way of avoiding the drawbacks of previous attempts was also suggested. It was pointed out that the standard way of solving for the coherent scattering amplitude $f_c(E)$ does not respect symmetry properties of the CPA effective medium, step by step during the iteration procedure, when the scattering matrices involved are not diagonal. This occurs, in the angular momentum representation, for cubic systems if one takes into account scattering channels for $l_{max} > 2$ in the Schrödinger case or for $l_{max} \geqslant 2$ in the Dirac case.

In studying light alloys it was not always necessary to allow for $l_{max} > 2$ and relativistic effects might be ignored without causing many errors, so that this drawback did not arise until heavy element alloys were considered. We shall briefly summarise the work of I in a following section, but here we simply stress that imposing such a symmetry condition during the iteration procedure is not merely convenient but also corresponds to a very precise physical constraint. As a result a reliable numerical scheme for solving the RKKR–CPA equations has been designed which has been applied to the $Cu_{0.75}$–$Au_{0.25}$ random alloy. The well behaved convergence properties of the new method and the agreement found with experimental data gave us confidence that it should now be possible to implement a SCF–RKKR–CPA scheme on the same footing as its non-relativistic analogue Before proceeding along that road, however, it is worthwhile investigating the extent to which the proposed scheme works in a similar manner as the non-relativistic method was tested in the past (Temmermann *et al* 1978, Pindor *et al* 1980) for light alloys.

As mentioned above, early attempts to find solutions of the RKKR–CPA equations failed in some cases: the Pd–Pt disordered alloy represents an example of such a situation. This circumstance, together with the intrinsic interest in these alloys, makes this system a good candidate to be studied using this new procedure.

In the next section we briefly recall the relevant equations of the RKKR–CPA approach and the method of solution we use. The third section will present a study of several Pd_c–Pt_{1-c} alloys, with an analysis which focuses in particular on the 'new' disorder that the CPA medium shows with respect to mass–velocity, Darwin and spin–orbit corrections.

2. Theoretical framework

It is well known that the study of the electronic properties of disordered systems poses us with the problem of performing ensemble averages of the relevant physical observables. In the mean-field approximation and by using a single-site approach within the multiple scattering framework, such a problem was solved in terms of the so called KKR–CPA (Stocks *et al* 1978). Later its relativistic generalisation (Staunton *et al* 1980) was also set out and the theoretical framework developed (Staunton *et al* 1983, Ebert *et al* 1985). In summary, the 'on energy shell' site diagonal matrix elements of the scattering path operator, $\tau_c^{ii}(E)$ for the 'coherent' lattice, and the corresponding single-site transition matrix $t_c(E)$ are determined. Such a result might be obtained by solving the following equations self-consistently:

$$\tau^{ii}_{c\gamma\gamma'}(E) = \frac{1}{\Omega_{BZ}} \int \tau_{c\gamma\gamma'}(\boldsymbol{q}, E)\, \mathrm{d}\boldsymbol{q} = \frac{1}{\Omega_{BZ}} \int (t_c^{-1}(E) - G(\boldsymbol{q}, E))^{-1}_{\gamma\gamma'}\, \mathrm{d}\boldsymbol{q} \tag{1}$$

$$t^{-1}_{c\gamma\gamma'}(E) = ct^{-1}_{A\gamma\gamma'}(E) - (1-c)t^{-1}_{B\gamma\gamma'}(E) + [(t_c^{-1}(E) - t_A^{-1}(E))\tau_c^{ii}(E)(t_c^{-1}(E) - t_B^{-1}(E))]_{\gamma\gamma'} \tag{2}$$

where $\gamma = \Gamma_n, \kappa$ labels the nth irreducible representation of the cubic double point

group, κ is the spin angular quantum number and the subscript A (B) indicates the alloy components. The relativistic KKR structure constants $G(\boldsymbol{q}, E)_{\gamma\gamma'}$ can be written as a linear combination of the non-relativistic ones (Onodera and Okazaki 1966). There are alternatives to equation (2): one is the usual form of the CPA condition:

$$c\tau_{A\gamma\gamma'} + (1-c)\tau_{B\gamma\gamma'} = \tau_{c\gamma\gamma'} \tag{3}$$

where

$$\tau_{\alpha\gamma\gamma'} = (D_\alpha \tau_c)_{\gamma\gamma'} = (\tau_c \tilde{D}_\alpha)_{\gamma\gamma'} \qquad (\alpha = A, B) \tag{4}$$

with the 'CPA projector' (Durham *et al* 1980) given by

$$D_{\alpha\gamma\gamma'}(E) = [1 + \tau_c(E)(t_\alpha^{-1}(E) - t_c^{-1}(E))]^{-1}_{\gamma\gamma'} \tag{5}$$

and

$$\tilde{D}_{\alpha\gamma\gamma'}(E) = [1 + (t_\alpha^{-1}(E) - t_c^{-1}(E))\tau_c(E)]^{-1}_{\gamma\gamma'}. \tag{6}$$

It turns out that, unlike τ_c, τ_α and t_c, the matrices D_α are not symmetric.

Another form of the CPA condition is, in terms of the excess of scattering operator X_α:

$$cX_{A\gamma\gamma'} + (1-c)X_{B\gamma\gamma'} = 0 \tag{7}$$

with

$$X_{\alpha\gamma\gamma'}(E) = [(t_\alpha^{-1}(E) - t_c^{-1}(E))^{-1} - \tau_c(E)]^{-1}. \tag{8}$$

As was stressed in I, the important point to note is that equations (2) and (7) are entirely equivalent only if they are solved *exactly*. This is not the case when, at some stage during the iterative procedure for solving CPA equations, equation (2) gives a t matrix which does not transform as the irreducible representation of the double point group. As was suggested by some authors (Pinski *et al* 1988), by defining

$$cX^n_{A\gamma\gamma'} + (1-c)X^n_{B\gamma\gamma'} = X^n_{c\gamma\gamma'} \neq 0, \tag{9}$$

where n labels the current iteration step, one can recognise that X_c^n may be related to the difference between two successive values of $t^{-1}_{c\gamma\gamma'}$, i.e.

$$X^n_{c\gamma\gamma'} = [(t_c^{-1,n} - t_c^{-1,n+1})^{-1} - \tau_c(t_c^{-1,n})]^{-1}_{\gamma\gamma'} \tag{10}$$

so that

$$t^{-1,n+1}_{c\gamma\gamma'} = t^{-1,n}_{c\gamma\gamma'} - [X_c^{-1,n} + \tau_c(t_c^{-1,n})]^{-1}_{\gamma\gamma'}. \tag{11}$$

Equating equations (9) and (10) is the key step to the solution of the RKKR–CPA numerical problem. The reason lies in the fact that such a scheme, as is possible to prove (Mills *et al* 1983), converges both in the 'weak' and 'strong' scattering limits provided that the initial guess is the single-site average t matrix (ATA). As often happens, for heavy-metal alloys the scattering can be strong in the d and s channels and weak in the p ones. The former numerical schemes used (e.g. the Newton–Raphson method) are effective in only one of these limits. Moreover, in I it was also shown numerically that the new scheme has the correct non-relativistic limit. Of course, owing to the increased dimensions of the matrices involved, the required computing time is increased with respect to the non-relativistic scheme. Despite this, we believe that the present procedure can be used to develop an efficient code and implement the full SCF–RKKR–CPA calculation.

Once $t_{c,\gamma\gamma'}$ and $\tau_{c,\gamma\gamma'}$ have been determined to a chosen tolerance, the electronic structure can be studied. In particular, we can compute the Bloch spectral function $A_B(\boldsymbol{q}, E)$ defined as (Faulkner and Stocks 1980)

$$n(E) = \frac{1}{\Omega_{BZ}} \int A_B(\boldsymbol{q}, E)\, d\boldsymbol{q} = -\frac{1}{\pi} \operatorname{Im} \operatorname{Tr} F^c(E)\tau_c(E) \tag{12}$$

where $n(E)$ is the electronic density of states and

$$A_B(\boldsymbol{q}, E) = -\frac{1}{\pi} \operatorname{Im} \operatorname{Tr}\big(F^{cc}(E)(\tau_c(\boldsymbol{q}, E) - \tau_c(E)) + F^c(E)\tau_c(E)\big). \tag{13}$$

Equation (13) can be written in order to display the contributions of the different species as

$$A_B(\boldsymbol{q}, E) = A_B^A(\boldsymbol{q}, E) + A_B^B(\boldsymbol{q}, E) + A_B^{AB}(\boldsymbol{q}, E) \tag{14}$$

where

$$A_B^\alpha(\boldsymbol{q}, E) = -\frac{1}{\pi} \operatorname{Im} \operatorname{Tr}\big(F^{\alpha\alpha}(E)(\tau_c(\boldsymbol{q}, E) - \tau_c(E)) + F^\alpha(E)\tau_c(E)\big) \tag{15}$$

$$A_B^{AB}(\boldsymbol{q}, E) = -\frac{1}{\pi} \operatorname{Im} \operatorname{Tr}[(F^{AB}(E) + F^{BA}(E))(\tau_c(\boldsymbol{q}, E) - \tau_c(E))] \tag{16}$$

$$F^\alpha(E) = c_\alpha Z^{\alpha\alpha}(E) D_\alpha(E) \tag{17}$$

$$F^{\alpha\beta}(E) = c_\alpha c_\beta \tilde{D}_\alpha(E) Z^{\alpha\beta}(E) D_\beta(E) \tag{18}$$

$$Z^{\alpha\beta}_{\gamma\gamma'}(E) = \int_{uc} R^\alpha_\gamma(\boldsymbol{r}, E) R^\beta_{\gamma'}(\boldsymbol{r}, E)\, d\boldsymbol{r}. \tag{19}$$

The wavefunctions $R^{\alpha(\beta)}_\gamma(\boldsymbol{r}, E)$ in equation (19), are 4-spinors normalised so that they join smoothly to their asymptotic form (Faulkner and Stocks 1980).

By searching for the peaks of the Bloch spectral function either as a function of $\boldsymbol{q}$ or E one can picture the 'bands' of the alloys provided the corresponding widths are small on the scale of their separations. Under the same conditions one can also define the Fermi surface as the locus of the peaks of $A_B(\boldsymbol{q}, E_F)$ and plot it along chosen directions of the Brillouin zone.

3. Results and discussion

The Pd–Pt system forms an FCC solid solution on the whole range of compositions and, as we mentioned above, the former attempts to compute the alloys' relativistic electronic structures failed owing to the lack of a reliable convergence procedure. We have applied our new scheme to a number of alloys and we found convergence in all situations.

The Pd and Pt atomic potentials were computed from relativistic Hartree–Fock–Slater charge densities for the neutral atom. Such potentials were then used to obtain the muffin-tin potentials $V_{MT}^{A(B)}$ for each species in the alloy with proper composition and lattice parameter. An open point of discussion is to state how good such potentials are in describing the physical properties of this alloy. Of course, charge self-consistent potentials are highly desirable, but at present we must be happy to use potentials built

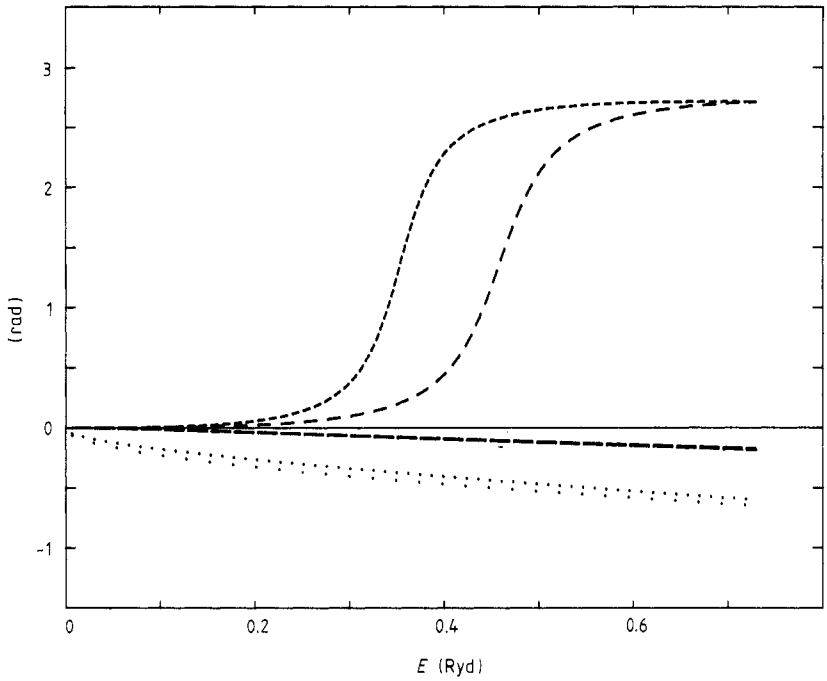

Figure 1. Non-relativistic scattering phase shifts for the $Pd_{0.7}$–$Pt_{0.3}$ alloy: dotted curves, $l = 0$ phase shift; short broken curves, $l = 1$ phase shift; long broken curves, $l = 2$ phase shift. The full line is an eye-guide for the ordinate zero. Large spaces are for Pd site phase shifts, close spaces for Pt. $l = 1$ phase shifts are not distinguishable.

following old band structure prescriptions for the pure components (Andersen 1970). From $V_{MT}^{A(B)}$ the phase shifts and the corresponding matrices $t_{A(B)\gamma\gamma'}$ can be computed straightforwardly and used to construct the ATA initial guess for the RKKR–CPA scheme.

For the sake of completeness we studied also the non-relativistic electronic structure of $Pd_{0.7}$–$Pt_{0.3}$. The relevant phase shifts are shown in figure 1. As can be seen, the d-resonance widths are large compared with the separation of A and B, and one might expect a common band description to be applicable. This is indeed confirmed by figure 2, which shows the non-relativistic density of states of the same alloy and its partial A and B contributions. Here, the contributions of the two species largely overlap. As a consequence the total density of states does not show particularly new features in comparison with that of a canonical FCC DOS. Incidentally, such a behaviour might explain the Nordheim-like trend of the residual resistivity in these alloys (see, e.g., Mott and Jones 1936).

Let us consider what happens when the speed of light is kept at 137 au. Figure 3 shows the phase shifts $\delta_\kappa(E)$ for the same potentials as figure 1. A relevant change is given by the strong Darwin correction on the Pt s channel which becomes attractive over a large region of energy. Moreover, apart from the spin–orbit splitting of the p and d phase shifts, we can note that the d-channel scattering is sharpened and the resonances are shifted down to lower energies, in comparison with the non-relativistic case, particularly for Pt. This sharpening, together with a larger separation between the d resonances, arises from the mass–velocity corrections, and points towards a well defined split-band regime. Such an effect can easily be seen in the Argand plots (figure 4) by

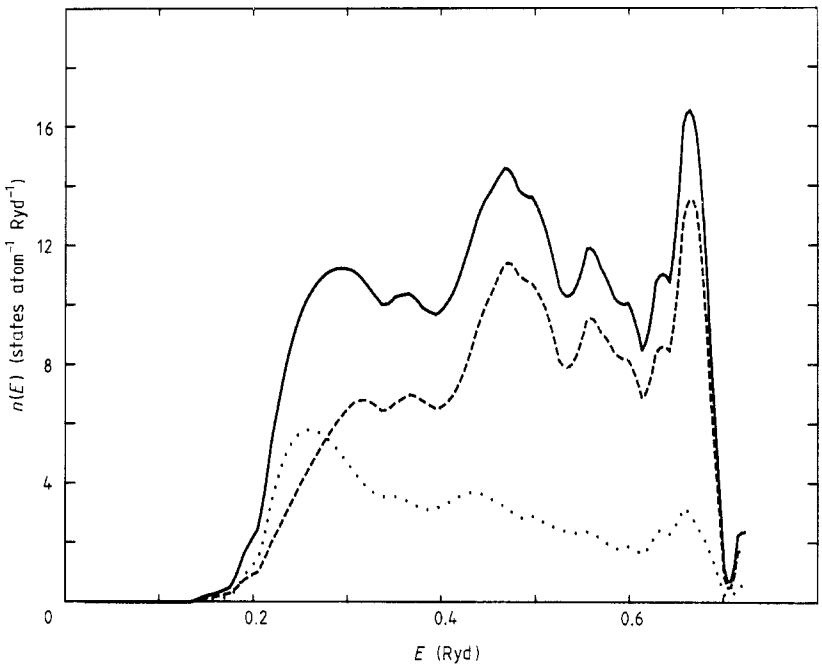

Figure 2. KKR–CPA local densities of states for $Pd_{0.7}$–$Pt_{0.3}$: dotted curve: Pt LDOS; broken curve: Pd LDOS; full curve: total DOS.

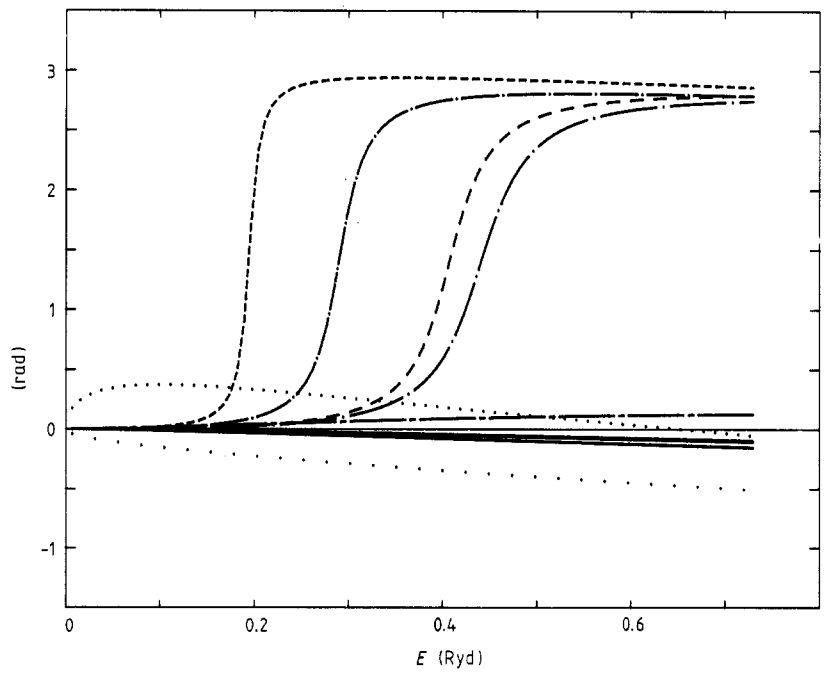

Figure 3. Relativistic scattering phase shifts for the $Pd_{0.7}$–$Pt_{0.3}$ alloy: dotted curves: $l = 0$, $j = \frac{1}{2}$ phase shifts; full curves: $l = 1$, $j = \frac{1}{2}, \frac{3}{2}$ phase shifts; chain curve: Pt, $l = 1$, $j = \frac{1}{2}$; broken curves: $l = 2$, $j = \frac{3}{2}$ phase shifts; short chain curves: $l = 2$, $j = \frac{5}{2}$ phase shifts. The continuous line is an eye-guide for the ordinate zero. Large spaces are for Pd, close spaces for Pt.

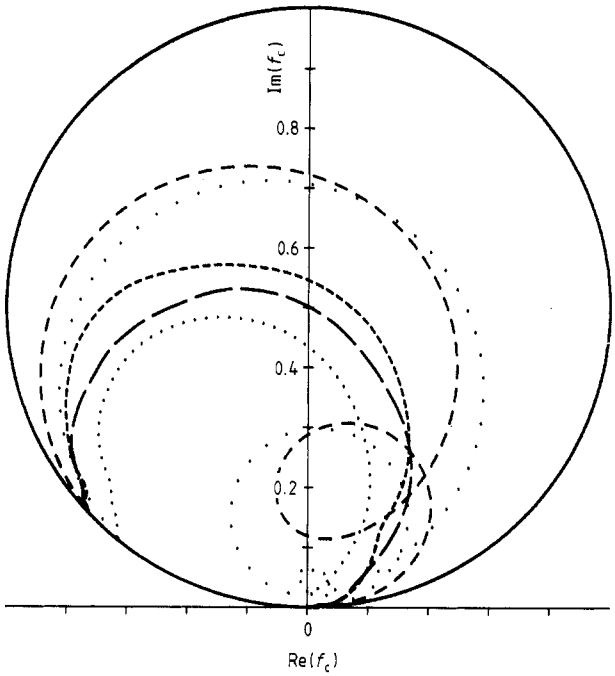

Figure 4. Argand plot for the d-like RCPA scattering amplitudes $c_{Pd} = 0.7$: dotted curve: $f^{CPA}_{-3\Gamma_7^+} = f^{ATA}_{-3\Gamma_8^+}$; large dotted line: $f^{ATA}_{2\Gamma_8^+}$; short broken curve: $f^{CPA}_{-3\Gamma_7^+}$; long broken curve (equally spaced): $f^{CPA}_{2\Gamma_8^+}$; long broken curve (unequally spaced): $f^{CPA}_{-3\Gamma_8^+}$.

looking at the ATA scattering amplitudes which clearly display the loops typical of a split-band situation. However, the CPA procedure tends to reduce this effect to give a more inelastic effective scatterer, whose amplitude is $f_{c\gamma\gamma'}(E)$. The corresponding densities of states are shown in figure 5. It is interesting to note that the main contributions of the partial DOS are well separated, giving a much more split-band-like picture than the non-relativistic case. In particular, the feature below 0.2 Ryd is quite well separated, unlike the corresponding non-relativistic situation. Such structure arises from the $Pt_{\Gamma_8^+}$ states which can be seen by looking at figure 6, where we show the band structures of hypothetical Pt and Pd 'pure' metals, each obtained by using the same muffin-tin potential of the $Pd_{0.7}$–$Pt_{0.3}$ alloy and referred to the same muffin-tin zero.

Figure 7 shows the total densities of states as a function of the concentration for $c = 0.3$ up to $c = 0.7$. All the curves are lined up at the muffin-tin zero, and one can see the increase in the bandwidths as platinum content grows. This is a consequence of the increase in atomic weight, and therefore spin–orbit coupling, and leads to a splitting of the Γ_7^+ and Γ_8^+ features in the Pt-rich alloys.

A more direct analysis can be carried out via the results shown in figure 8, where the 'component' contributions to the Bloch spectral functions (see equation (15)) at the Γ point for the $c = 0.70$ alloy are plotted. Here it is clearly seen that the 'd bands' are essentially separated, apart from the region in the middle of the spectrum, and that the cross contribution tends to squeeze the d band as a whole. In figure 9 we plot the function $A_B(\boldsymbol{q}, E)$ along the Δ line in the Brillouin zone for $c = 0.70$. Note that the peak on the

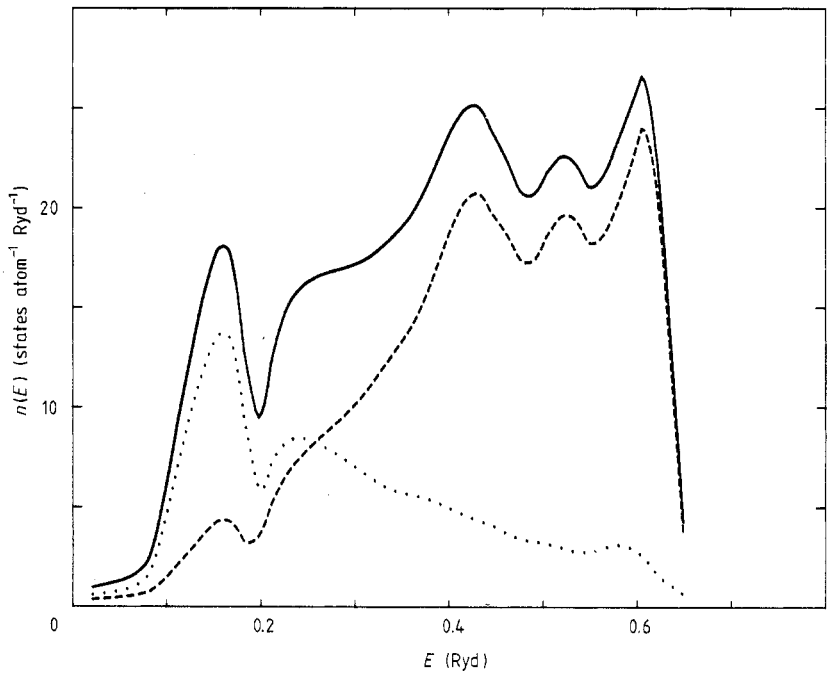

Figure 5. Relativistic KKR–CPA local densities of states for $c_{Pd} = 0.7$. Notation as in figure 2.

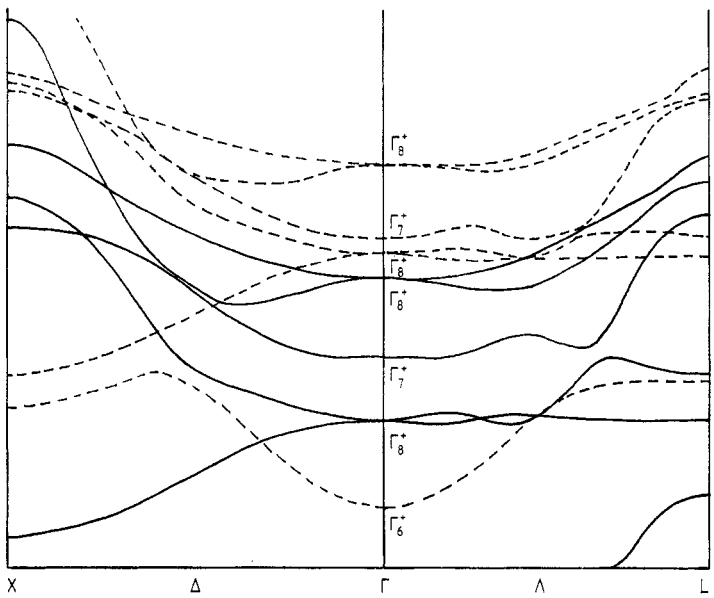

Figure 6. Relativistic KKR band structures for the potentials corresponding to the $Pd_{0.7}$–$Pt_{0.3}$ alloy: broken curves, Pd; full curves, Pt.

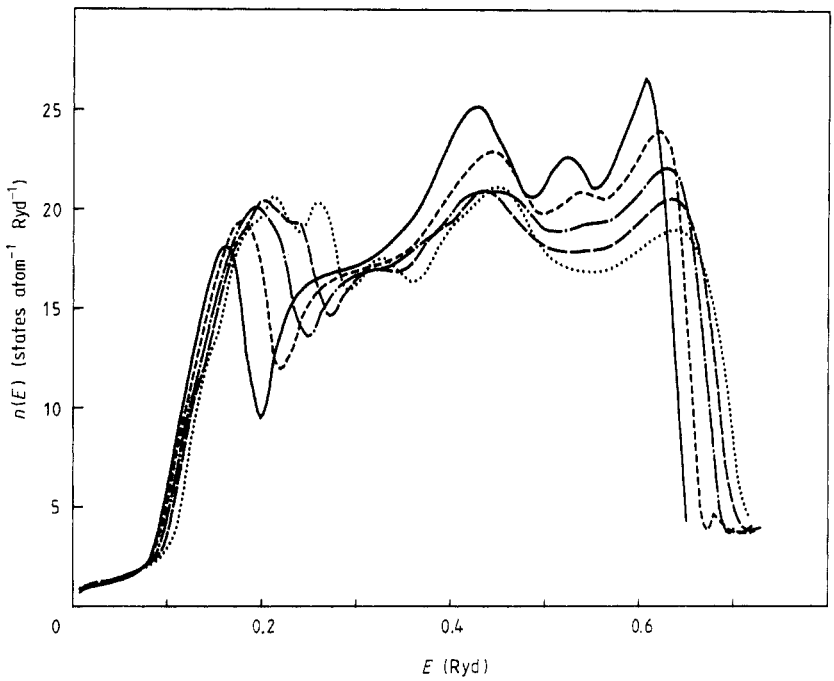

Figure 7. Density of electronic states for several palladium concentrations: full curve, c = 0.3; short broken curve, c = 0.4; chain curve, c = 0.5; long broken curve, c = 0.6; dotted curve, c = 0.7.

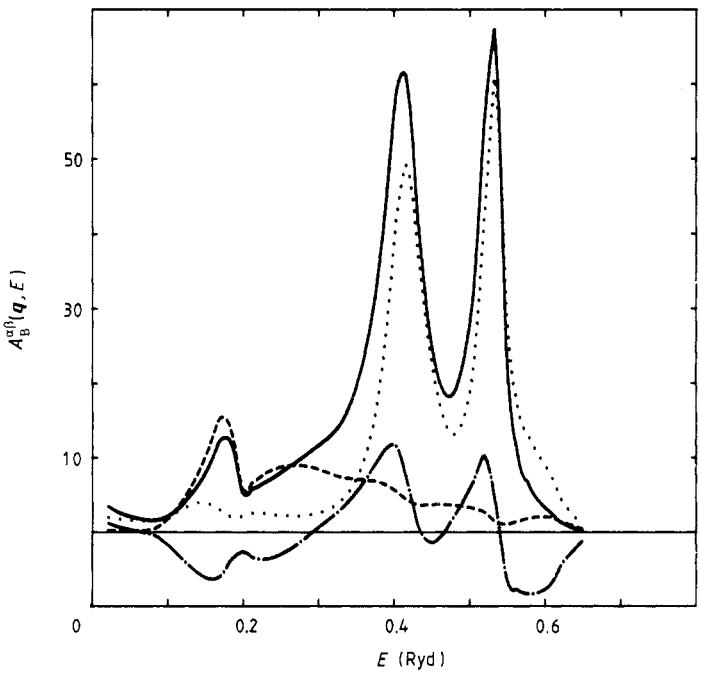

Figure 8. Bloch spectral function and its A, B and AB components at the Γ point in the Brillouin zone for the c = 0.3 alloy: broken curve, Pt component; dotted curve, Pd component; chain curve, 'AB' component; full curve, total.

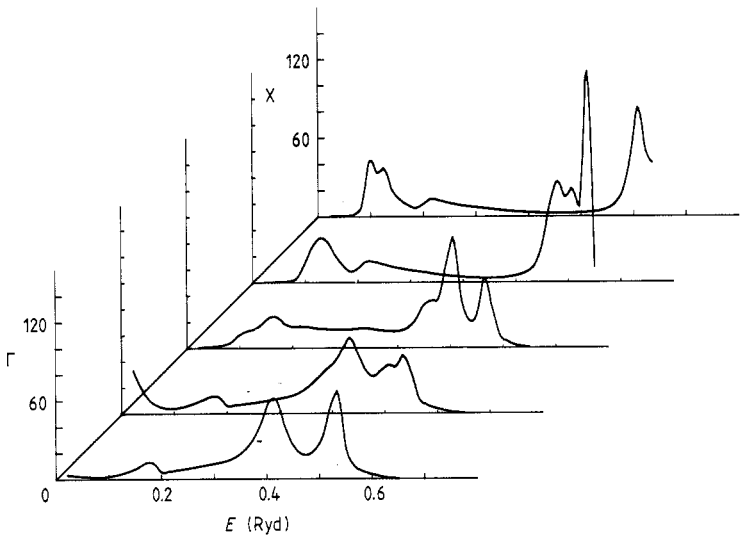

Figure 9. Bloch spectral functions along the Δ direction in the Brillouin zone for the c_{Pd} = 0.7 alloy: $\boldsymbol{k}$ points are equispaced from Γ to X.

high-energy side, a related Pd feature, has become quite sharp in crossing the Fermi level. We found the same behaviour in all the directions studied and for all the alloys investigated. This circumstance allows a Fermi surface to be defined despite the large damping of the states below E_F. We mapped out the peaks of $A_B(\boldsymbol{q}, E_F)$ on the ΓKLXWK planes and the results are shown in figure 10. The topology of the Fermi surface resembles that of the pure metals very much (Andersen 1970), as one should expect, keeping in mind that the Fermi level lies near the top of the d band where the states are essentially Pd related. In this energy region the influence of the alloying is consequently small. It is this circumstance which may be responsible for the Nordheim behaviour of the residual resistivity mentioned earlier.

The relativistic and non-relativistic calculations presented here are directly comparable because they were performed within the same accuracy, the only difference being the use of the Dirac or Schrödinger equation and the double or single point group representation. A good numerical check for relativistic results was to set c, the velocity of light, to a very large value, and we found that figures 3 and 5 reduced to figures 1 and 2 within the required tolerance. This shows that we have dealt with the Dirac and Schrödinger problems on an equal footing.

4. Conclusions

In summary, even though our predictions would only be quantitative if we had applied a fully charge self-consistent treatment (SCF–RKKR–CPA) to the problem, we believe that the results above are physically interesting and instructive and, in particular, that they give insight into the way that the CPA is able to deal with relativistic effects on an equal footing with the non-relativistic counterparts. Moreover, we have shown that the method

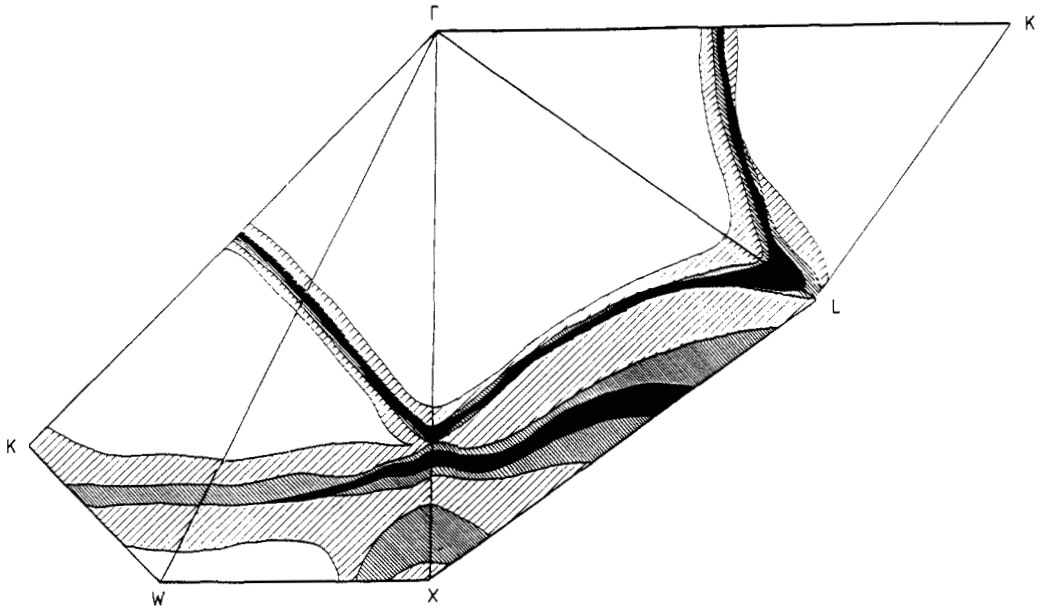

Figure 10. 'Fermi surface' for the $c_{Pd} = 0.3$ alloy. Open regions, $\boldsymbol{k}$ points of the symmetry faces indicated where the value of the spectral function is less than 10; wide hatched regions, as before but $10 < A_B(\boldsymbol{q}, E_F) < 40$; close hatched regions, $40 < A_B(\boldsymbol{q}, E_F) < 60$; solid regions, $A_B(\boldsymbol{q}, E_F) > 60$.

employed, and the computer code used, reveal the way of achieving such a SCF–RKKR–CPA scheme with the same reliability as the existing non-relativistic analogue.

Of course, we are aware that the results we have presented should be tested by a detailed comparison with experimental data, which unfortunately are lacking in the literature up to now. We hope our calculations will focus new experimental interest on this system.

Acknowledgments

The authors wish to acknowledge the CRRN–SM Committee for financial support obtained. We have also benefited from the use of the CRAY–XMP facilities of the CINECA Computing Centre, where most of the calculations were performed, through support from the Consiglio Nazionale delle Ricerche (Italy).

References

Andersen O K 1970 *Phys. Rev.* B **2** 883
Durham P J, Gyorffy B L and Pindor A J 1980 *J. Phys. F: Met. Phys.* **9** 661
Ebert H, Weinberger P and Voitlander J 1985 *Phys. Rev.* B **31** 7557
Faulkner J S and Stocks G M 1980 *Phys. Rev.* B **21** 3227
Ginatempo B and Staunton J B 1988 *J. Phys. F: Met. Phys.* **18** 1827
Gyorffy B L, Johnson D D, Pinski F J, Nicholson D M and Stocks G M 1989 *Alloy Phase Stability* ed. G M Stocks and A Gonis (NATO–ASI Series) Dordrecht: Kluwer Academic) p 421

Johnson D D, Pinski F J and Stocks G M 1984 *Phys. Rev.* B **30** 5508
Mills R, Gray L J and Kaplan T 1983 *Phys. Rev.* B **27** 3252
Mott N F and Jones H 1936 *The Theory of the Properties of Metals and Alloys* (Oxford: Oxford University Press)
Onodera Y and Okazaki M 1966 *J. Phys. Soc. Japan* **21** 2400
Pindor A J, Temmermann W M, Gyorffy B L and Stocks G M 1980 *J. Phys. F: Met. Phys.* **10** 2617
Pinski F J, Nicholson D M, Stocks G M, Butler W H, Johnson D D and Gyorffy B L 1988 *Proc. 3rd Int. Conf. on Supercomputing (Supercomputing '88)* vol 1, ed. L P Kartashev and S I Kartashev (Boston: International Supercomputing Institute Inc.) p 321
Staunton J B, Gyorffy B L and Weinberger P 1980 *J. Phys. F: Met. Phys.* **10** 2665
Staunton J B, Weinberger P and Gyorffy B L 1983 *J. Phys. F: Met. Phys.* **13** 779
Stocks G M and Gonis A (eds) 1989 *Alloy Phase Stability* (NATO-ASI Series) (Dordrecht: Kluwer Academic)
Stocks G M, Temmermann W M and Gyorffy B L 1978 *Phys. Rev. Lett.* **41** 339
Stocks G M and Winter H 1982 *Z. Phys.* B **46** 95
Temmermann W M, Gyorffy B L and Stocks G M 1978 *J. Phys. F: Met. Phys.* **8** 2461
Wadsworth J, Gyorffy B L and Stocks G M 1985 *High Temperature Alloys: Theory and Design* ed. J O Stiegler (Warrendale, PA: AIME) p 183